# General approach for partitioning and phase separation in macromolecular coexisting phases

Vikki Anand Varma and Alberto Scacchi*
*Department of Mechanical and Materials Engineering, University of Turku, Vesilinnantie 5, FI-20014 Turku, Finland*

(Received 6 December 2025; accepted 19 May 2026; published 16 June 2026)

Partitioning of (bio)materials in polymeric mixtures is a key phenomenon both in cellular environments, as well as in industrial applications. In cells, macromolecules are distributed among distinct biomolecular phases. The coexistence of polymeric aqueous phases in multicomponent systems has been widely exploited for the extraction and purification of (bio)materials from aqueous environments. Despite their relevance, key physical and chemical properties controlling the phase behavior of these complex systems are still lacking. Here, we have developed a classical density functional theory approach for describing the phase coexistence and partitioning of an arbitrary number of polymers and suspended materials. As a case example, we focus on a binary mixture of phase separating polymers in which a third material is dispersed. We explore the effect of size ratios and affinities between the different materials and address their distribution and coexisting densities, and find optimal conditions for partitioning.

DOI: 10.1103/v6nd-87cd

## I. INTRODUCTION

Partitioning within phase separating systems is fundamental to many everyday processes. Notable examples are cellular processes. Inside cells, liquid–liquid phase separation occurs alongside the presence of various biomaterials (colloidal or polymeric components) that are dispersed throughout the environment [1–3]. These components can partition differently depending on their chemical and physical properties, influencing cellular organization and function [4]. Controlling partitioning within liquid-liquid phase separation also offers a platform for bioengineering [5,6]. Several developments for bioinspired materials require control of the partitioning of different species within liquid-phases [7]. On a larger scale, so-called aqueous two-phase systems (ATPSs) have been proposed as an alternative to more conventional water purification methods [8,9].

Despite the ubiquity of this process, a comprehensive understanding of the chemical and physical factors governing phase behavior in such complex systems remains limited, as responses often vary in a highly system-dependent manner.

Coarse-grained particle-based simulations have recently been employed to investigate the partitioning of magnetic nanoparticles within a binary mixture of demixing polymers [10]. This approach provides valuable insights into molecular-level interactions and self-organization within specific systems. However, when the goal is to systematically explore a broad landscape of chemically and physically distinct scenarios, such simulations become increasingly demanding in terms of computational time and resources. Because of this, here we develop an approach based on classical density functional theory (cDFT) [11–13] able to describe the phase response of an arbitrary number of polymers and suspended materials.

cDFT relies on the minimization of a free-energy functional. A central challenge lies in identifying or constructing a functional that accurately captures the physical behavior of the system under study. Over the past several decades, significant effort has been devoted to both the development of new functionals and the refinement of existing ones (for reviews, see [14–16]). Here, we combine fundamental measure theory (FMT) [17], free volume (FV) theory [18], and mean field (MF) theory [19] for obtaining the coexisting densities. In addition to using the standard MF (SMF) formalism as benchmark, we propose an enhanced MF (EMF) alternative that explicitly considers the effective free volume available to the different components. To study inhomogeneous cases, we combine the Asakura-Osawa-Vrij (AOV) model [20] given for the model polymer within the framework of FMT, with our EMF formalism. We demonstrate the applicability of our approach by tackling a representative case from aqueous two-phase systems used in water purification from pollutants [21], as well as for biomaterial purification [22], where two immiscible polymers phase separate in the presence of a third dispersed material. Other relevant applications of these systems involve, e.g., the investigation of ultralow interfacial tension and micropattern formation in ferrofluids [23], as well as their utilization in cell-mimicking microrobotic systems [24]. More broadly, our findings can be extended to other systems, such as biomolecular condensates [25] containing, e.g., dispersed globular proteins or viruslike particles.

Our work is structured as follows. In Sec. II A, we define the interaction potentials among different species. In Sec. II B, we introduce free-energy functionals for a multicomponent polymer-colloid mixture in bulk. In Sec. II C, we propose a general scheme to determine coexisting densities for a given

*Contact author: alberto.scacchi@utu.fi

*Published by the American Physical Society under the terms of the Creative Commons Attribution 4.0 International license. Further distribution of this work must maintain attribution to the author(s) and the published article's title, journal citation, and DOI.*

multicomponent and multiphase grand canonical ensemble. In Sec. II D, we extend the free-energy functionals to address inhomogeneous systems. In Sec. III A, we consider a specific case, namely, two immiscible polymers and a dispersed colloid, and study its bulk response under different conditions, such as polymer size, affinity, and densities. Then, in Sec. III B, we study inhomogeneous properties of the same ternary mixture considered in bulk. In both Secs. III A and III B, a brief comparison with particle-based simulations is presented. Finally, in Sec. IV, we summarize our findings and discuss the limitations and possible extensions of our approach.

## II. THEORY AND IMPLEMENTATION

Our scheme relies on splitting any interaction potential into a soft (either attractive or repulsive) part and a hard-core repulsive part [26–29]. The soft interactions are treated within a MF approximation, while the hard-core repulsion is handled using established methods within the cDFT framework, as described in detail below.

### A. Interaction potential

#### 1. Polymer-polymer interaction

Polymers are described by Gaussian potentials of the form

$$\phi_{pq}(r) = \epsilon_{pq} e^{-(\frac{r}{R_{pq}})^2}, \tag{1}$$

where $p, q \in \{1, \ldots, \mathrm{n}\}$, and n represents the total number of polymer species in the system. Throughout, all energies, including $\epsilon_{pq} > 0$, are expressed in units of $k_\mathrm{B}T$, where $k_\mathrm{B}$ is the Boltzmann constant and $T$ the temperature of the system. $\epsilon_{pq}$ describes the repulsion strength between different types of polymers, controlling both species miscibility and polymer solvophilicities. Finally, $R_{pp}$ is a measure of the radius of gyration of each polymer species. To calculate the interspecies radii, we use the standard quadratic mean relation

$$R_{pq}^2 = \frac{R_{pp}^2 + R_{qq}^2}{2}, \tag{2}$$

which is based on the convolution of Gaussian functions. The potential in Eq. (1) is well suited to describe the effective interaction between both linear polymers and dendrimers in good solvents [30–34]. This and similar interaction potentials have been used extensively in the context of cDFT for polymers (see, e.g., [35–37]).

#### 2. Colloid-colloid interaction

Colloidal particles are modeled as hard spheres, i.e.,

$$\phi_{cd}(r) = \begin{cases} +\infty & r < \sigma_{cd} \\ 0 & r \geqslant \sigma_{cd}, \end{cases} \tag{3}$$

where $c, d \in \{\mathrm{n}+1, \ldots, \mathrm{n}+\mathrm{m}\}$, with m representing the total number of colloidal species. $\sigma_{cc}$ is the diameter of the spherical colloids, while the cross-diameter $\sigma_{cd} = (\sigma_{cc} + \sigma_{dd})/2$ (additive colloidal mixture).

An attractive interaction between colloids can, in principle, be included within a mean-field treatment. For simplicity, however, we omit it here.

#### 3. Colloid-polymer interaction

The colloid-polymer interaction is split into two parts. The first models depletion forces via a hardcore repulsive potential, reading

$$\phi_{cp}^{\mathrm{rep}}(r) = \begin{cases} +\infty, & r < \sigma_{cp} \\ 0, & r \geqslant \sigma_{cp}, \end{cases} \tag{4}$$

where $\sigma_{cp} = (\sigma_{pp} + \sigma_{cc})/2$, and $\sigma_{pp}$ represents the excluded volume effect of the polymers in the presence of colloids (see discussion on free energy for hardcore interaction in Sec. II B). The second, describing surface attraction (e.g. due to electrostatic or solvophobic interactions), is defined as

$$\phi_{cp}^{\mathrm{att}}(r) = \begin{cases} 0, & r < \sigma_{cp} \\ -\epsilon_{cp}, & \sigma_{cp} \leqslant r < \delta\sigma_{cp} \\ 0, & r \geqslant \delta\sigma_{cp}, \end{cases} \tag{5}$$

where $\delta > 1$ sets the range and $\epsilon_{cp}$ the strength of the attraction, respectively.

### B. Free-energy functional for bulk system

We start by defining the Helmholtz free-energy functional per unit volume of a system with n polymers and m colloids. Generally, it can be written as the sum of the ideal and the excess contributions [11], i.e.,

$$\mathcal{F}[\{\rho_i\}] = \mathcal{F}_{\mathrm{id}}[\{\rho_i\}] + \mathcal{F}_{\mathrm{exc}}[\{\rho_i\}], \tag{6}$$

where the ideal term takes the known form

$$\beta\mathcal{F}_{\mathrm{id}}[\{\rho_i\}] = \sum_i \left[\rho_i \ln\left(\Lambda_i^3 \rho_i\right) - \rho_i\right], \tag{7}$$

where $i \in \{1, ..., \mathrm{n}+\mathrm{m}\}$, $\rho_i$ is the number density of species $i$, $\beta = (k_\mathrm{B}T)^{-1}$, and $\Lambda_i$ is the de Broglie wavelength. We express the excess free energy as

$$\mathcal{F}_{\mathrm{exc}}[\{\rho_i\}] = \mathcal{F}_{\mathrm{HC}}[\{\rho_i\}] + \mathcal{F}_{\mathrm{FV}}[\{\rho_i\}] + \mathcal{F}_{\mathrm{EMF}}[\{\rho_i\}]. \tag{8}$$

This splitting is approximate and follows a physically motivated ansatz [11,14]. The first term, $\mathcal{F}_{\mathrm{HC}}$, describes all hardcore contributions which rise from colloid-colloid interactions, Eq. (3). In this case, the only relevant densities correspond to $i \in \{\mathrm{n}+1, \ldots, \mathrm{n}+\mathrm{m}\}$. The free volume term, $\mathcal{F}_{\mathrm{FV}}$, takes care of the depletion forces arising from colloid-polymer interactions [Eq. (4)]. Finally, the EMF term, $\mathcal{F}_{\mathrm{EMF}}$, describes the interactions between all polymers [Eq. (1)], as well as of the attractive contribution of the colloid-polymer interactions, Eq. (5).

#### 1. Free energy for hardcore interaction

For calculating the coexisting densities of a phase separating system, one can focus on expressing the free energy for homogeneous systems. In this case, $\mathcal{F}_{\mathrm{HC}}$ can be expressed using the Rosenfeld's approximation [17], which is very accurate within low density regimes. The latter reads [38]

$$\beta\mathcal{F}_{\mathrm{HC}}[\{\rho_i\}] = -n_0 \ln(1-n_3) + \frac{n_1 n_2}{1-n_3} + \frac{1}{24\pi}\frac{n_2^3}{(1-n_3)^2}, \tag{9}$$

where the weighted densities are summed over the colloidal species only. For a homogeneous mixture of colloids, the scalar weighted densities can be expressed directly in terms of the colloidal number densities as

$$n_0 = \sum_{i=\mathrm{n}+1}^{\mathrm{n}+\mathrm{m}} \rho_i, \quad n_1 = \sum_{i=\mathrm{n}+1}^{\mathrm{n}+\mathrm{m}} R_i \rho_i, \\ n_2 = \sum_{i=\mathrm{n}+1}^{\mathrm{n}+\mathrm{m}} 4\pi R_i^2 \rho_i, \quad n_3 = \sum_{i=\mathrm{n}+1}^{\mathrm{n}+\mathrm{m}} \frac{4}{3}\pi R_i^3 \rho_i. \tag{10}$$

Here, $R_i$ denotes the radius of the $i$th colloidal species.

Polymers act as depletants for all colloidal species due to an effective reduction of the accessible volume. This effect can be included by means of the FV theory [18]. The latter considers the cost of inserting a polymer at a given chemical potential for a specific density of colloids, and is given by

$$\beta \mathcal{F}_{\mathrm{FV}}[\{\rho_i\}] = -\sum_p \rho_p \ln \alpha_p, \tag{11}$$

where $\alpha_p$ depends upon the polymers' and colloids' shape and size. For a particular total colloidal packing fraction $\eta = \sum_c \eta_c = \sum_c \rho_c \sigma_{cc}^3 \pi/6$, the general expression for $\alpha_p$ is given by [18]

$$\alpha_p = (1-\eta)\exp\left[-\frac{A_p(\{\rho_c\})}{(1-\eta)} - \frac{B_p(\{\rho_c\})}{(1-\eta)^2} - \frac{C_p(\{\rho_c\})}{(1-\eta)^3}\right]. \tag{12}$$

The coefficients $A_p(\{\rho_c\})$, $B_p(\{\rho_c\})$, and $C_p(\{\rho_c\})$ for the polymer species $p \in \{1, \ldots, \mathrm{n}\}$ are given by

$$A_p(\{\rho_c\}) = s_p \sum_c a_c \rho_c + a_p \sum_c s_c \rho_c + v_p \sum_c \rho_c, \tag{13}$$

$$B_p(\{\rho_c\}) = \frac{1}{2} s_p^2 \left(\sum_c \rho_c a_c\right)^2 + v_p \left(\sum_c s_c \rho_c\right)\left(\sum_c a_c \rho_c\right), \tag{14}$$

and

$$C_p(\{\rho_c\}) = \frac{1}{12\pi} v_p \left(\sum_c a_c \rho_c\right)^3, \tag{15}$$

where $a_i = \pi \sigma_{ii}^2$ represents the surface area, $s_i = \sigma_{ii}/2$ the radius, and $v_i = \frac{\pi}{6}\sigma_{ii}^3$ the volume of the particle, with $c \in \{\mathrm{n}+1, \ldots, \mathrm{n}+\mathrm{m}\}$ and $i \in \{1, \ldots, \mathrm{n}+\mathrm{m}\}$. $\sigma_{cp}$ corresponds to the minimum distance between the center of mass of polymer $p$ and the colloid $c$, which represents the excluded volume between a colloid and a polymer. Note that $\sigma_{pp}$ is often chosen as $\sigma_{pp} = R_{pp} + \frac{1}{2}\sigma_{cc}$ [20].

#### 2. *Free energy for soft interaction*

In the presence of colloids, polymers experience confinement due to the excluded volume arising from the presence of colloids. This is particularly important when the total amount of colloids is at relatively high value. As a consequence, the perturbative MF can underestimate pressure and free energy. Therefore, the effective polymer density has to be modified by a factor $\alpha_p'$, with $\alpha_p' \neq \alpha_p$ [39–42]. Specifically, $\alpha_p$ is the accessible volume which accounts for the restriction of the polymer center of mass within the excluded volume around colloids, while $\alpha_p'$ represents the actual volume available for the polymer body to occupy. Unlike $\alpha_p$, the form of $\alpha_p'$ is not known. The simplest estimate of $\alpha_p'$ can be obtained by writing the effective volume in terms of an expansion over $\eta$, i.e.,

$$V_p^{\mathrm{eff}} = V(1 - \beta_1 \eta + \beta_2 \eta^2 + \ldots). \tag{16}$$

Analogous to a van der Waals-type approximation [43], we write the effective free volume available to polymers as

$$V_p^{\mathrm{eff}} = V - \sum_c \left[\frac{1}{2} v_{cp} N_c - \frac{3}{8} v_{cp}^2 N_c^2\right], \tag{17}$$

where $v_{cp}$ is the apparent volume arising from steric interactions between colloid $c$ and polymer $p$, given by $v_{cp} = \frac{\pi}{6}\sigma_{cp}^3$. Equation (17) is obtained by considering $\beta_1 = \frac{1}{2}$ and $\beta_2 = \frac{3}{8}$ in Eq. (16), while replacing $v_{cc}$ (representing the volume of colloid $c$ in $\eta_c$) with $v_{cp}$. The latter assumption allows us to also take into account the size of the polymers explicitly. Under this assumption, the corresponding effective polymer density is

$$\rho_p' = \frac{N_p}{V_{\mathrm{eff}}} = \frac{N_p}{V - \sum_c \left(\frac{1}{2} v_{cp} N_c - \frac{3}{8} v_{cp}^2 N_c^2\right)} = \frac{\rho_p}{\alpha_p'}, \tag{18}$$

with

$$\alpha_p' = 1 - \sum_c \left[\frac{1}{2} v_{cp} \rho_c - \frac{3}{8} v_{cp}^2 \rho_c^2\right]. \tag{19}$$

Similarly, the presence of several colloidal species reduces the effective available volume to the individual colloidal species. Namely, for species $c$, we have

$$\alpha_c' = 1 - \sum_{d \neq c} \left[\frac{1}{2} v_{cd} \rho_d - \frac{3}{8} v_{cd}^2 \rho_d^2\right], \tag{20}$$

such that $c, d \in \{\mathrm{n}+1, ..., \mathrm{n}+\mathrm{m}\}$. In terms of these effective densities, the MF contribution to the bulk free energy due to polymer-polymer and polymer-colloids interaction is given by the EMF functional

$$\beta \mathcal{F}_{\mathrm{EMF}} = \frac{1}{2} \sum_{i,j} \alpha_i' \rho_i' \rho_j' \hat{V}_{ij}. \tag{21}$$

Note that the SMF functional is obtained by setting $\alpha_i' = 1$, $\forall i$, and replacing the effective densities with their original values, i.e.,

$$\beta \mathcal{F}_{\mathrm{SMF}} = \frac{1}{2} \sum_{i,j} \rho_i \rho_j \hat{V}_{ij}, \tag{22}$$

where $\hat{V}_{ij}$ are the integrated strengths [35] and where $i, j \in \{1, \ldots, \mathrm{n}+\mathrm{m}\}$. The factors $\alpha_i'$ ensure the correct normalization of particle numbers when integrating over the total volume of the system [44].

Since all interaction potentials here are isotropic, the integrated strength for any pair of species $i$ and $j$, is defined as [35,39]

$$\beta \hat{V}_{ij} = 4\pi \int r^2 \phi_{ij}(r) dr, \tag{23}$$

which, for a pair interaction defined by Eq. (1), can be expressed analytically as

$$\hat{V}_{pq} = \pi^{3/2} \epsilon_{pq} R_{pq}^3. \tag{24}$$

Hereafter, $\hat{V}_{pq}$ denotes the dimensionless quantity $\beta \hat{V}_{pq} \sigma^{-3}$, where $\sigma$ defines the unit of length.

### C. Coexistence criteria

The chemical potential for any species $i$ can be expressed as

$$\mu_i = -\frac{\partial \mathcal{F}}{\partial \rho_i}, \tag{25}$$

where $\mathcal{F}$ is the Helmholtz free energy per unit volume given in Eq. (6). The total pressure $P$, in the absence of any external potential, reads

$$P = -\mathcal{F} + \sum_i \mu_i \rho_i, \tag{26}$$

where the summation runs over all species.

Let us consider the existence of two coexisting phases, phase I and phase II. Following the Gibbs' criteria, the coexisting conditions are

$$T^{\mathrm{I}} = T^{\mathrm{II}}, \quad \mu_i^{\mathrm{I}} = \mu_i^{\mathrm{II}}, \quad \text{and} \quad P^{\mathrm{I}} = P^{\mathrm{II}}, \tag{27}$$

where $i \in \{1, \ldots, \mathrm{n} + \mathrm{m}\}$. Note that, in the present study, the temperature has been held constant throughout. Under these constraints, we are left with $\mathrm{n} + \mathrm{m} + 1$ equations to solve for $2(\mathrm{n} + \mathrm{m})$ variables, representing the coexisting densities of all species in the two phases. At this point, the system comprises fewer equations than unknowns, resulting in an underdetermined system and nonunique solutions. To solve this, one needs to add additional constraints. We fix the density of each species such that

$$V_{\mathrm{f}} \rho_i^{\mathrm{I}} + (1 - V_{\mathrm{f}}) \rho_i^{\mathrm{II}} = \bar{\rho}_i, \tag{28}$$

with

$$\bar{\rho}_i = N_i / V, \tag{29}$$

where $N_i$ is the total number of particles of species $i$, $V$ is the total volume of the system, and $\bar{\rho}_i$ the average density of species $i$. $V_{\mathrm{f}}$ is the volume fraction representing phase I, thus $(1 - V_{\mathrm{f}})$ represents the volume fraction of phase II. By doing so, we add an extra variable, $V_{\mathrm{f}}$, which provides $\mathrm{n} + \mathrm{m}$ new equations through (28). We are now left with $2(\mathrm{n} + \mathrm{m}) + 1$ equations and $2(\mathrm{n} + \mathrm{m}) + 1$ variables. While the present scheme illustrates the approach for a system exhibiting at most two coexisting phases, this does not represent a limitation of the method. In general, the formulation can be extended to systems with an arbitrary number of coexisting phases by considering volume-fraction variables $V_{\mathrm{f}}^k$ for $k = 1, \ldots, l$, corresponding to a total of $l + 1$ phases.

There are several approaches to determine coexistence densities and construct the binodal [35,45,46]. In the present formalism, we assume a given number of coexisting phases and fix the average density for all species within each phase. This reduces the coexistence problem to solving Eq. (27) and Eq. (28). Solving these equations directly in terms of the densities can be computationally demanding due to the large parameter space. To simplify the problem and achieve faster convergence, we express the species densities as fractions of the total particle density within each phase, given by

$$\rho_i = \rho_{\mathrm{t}} \times x_{i-1} \prod_{j=i}^{\mathrm{n+m-1}} x_j', \tag{30}$$

where $\rho_{\mathrm{t}} = \sum_i \rho_i$, $i \in \{1, \ldots, n + m\}$, $x_i \in [0, 1]$, $x_i' = 1 - x_i$, and $x_0, x_0' = 1$. This procedure is repeated for increasing numbers of candidate phases to determine the maximum number of stable coexisting phases. The corresponding reduced densities can be expressed as

$$x_i = \frac{\rho_{i+1}}{\sum_{j=1}^{i+1} \rho_j}. \tag{31}$$

This nested construction ensures that all species densities remain positive. The structure can be interpreted as a sequence of branching ratios, where each $x_i$ governs the split of remaining density among successive species. This representation is particularly well-suited for numerical optimization and phase coexistence solvers, as it transforms the constrained problem of non-negative, normalized densities into an unconstrained optimization over $\rho_{\mathrm{t}}$ and $\{x_i\} \in (0, 1)$. The proposed reformulation helps in restricting the solver to find a disjoint solution using simple numerical solving modules, such as, e.g., `hybr`, freely available in Python. The numerical approach consists of the following: one begins by generating a trial solution in terms of reduced densities. This trial solution is then transformed into real densities, which are substituted into the coexistence equations. The values are iteratively updated until convergence is achieved toward a disjoint solution in the reduced variables. Once convergence is confirmed, the solution is converted back into real densities. A detailed description of these steps is provided in Sec. II of the Supplemental Material (SM) [47].

Using this formulation, the chemical potential for the $i$th component can be written as

$$\mu_i = f + \rho_{\mathrm{t}} \frac{\partial f}{\partial \rho_{\mathrm{t}}} + \sum_{\substack{S \subseteq \{x_{i-1}, \ldots, x_{\mathrm{n+m-1}}\} \\ S \neq \emptyset}} \left( \frac{\partial^{|S|} f}{\prod_{x_j \in S} \partial x_j} \prod_{x_j \in S} w_j(x_j) \right), \tag{32}$$

where free energy per particle, $f$, is expressed in terms of reduced densities ($\{\rho_{\mathrm{t}}, x_1, \ldots, x_{\mathrm{n+m-1}}\}$ for an $\mathrm{n} + \mathrm{m}$-component system). $S \subseteq \{x_{i-1}, \ldots, x_{\mathrm{n+m-1}}\}$ represents summation performed over all the possible subsets (all possible combination of different number of species and their permutation). However all the elements must belong to the set $\{x_{i-1}, \ldots, x_{\mathrm{n+m-1}}\}$. $w_j(x_j)$ is given by

$$w_j(x_j) = \begin{cases} 1 - x_j, & \text{if } j = i \text{ and } i > 1 \\ -x_j, & \text{otherwise.} \end{cases} \tag{33}$$

Within this formulation, the pressure now reads

$$P = \rho_{\mathrm{t}}^2 \frac{\partial f}{\partial \rho_{\mathrm{t}}}. \tag{34}$$

### D. Grand potential for inhomogeneous systems

The grand canonical potential of an inhomogeneous system, $\Omega$, can be written as [11]

$$\Omega[\{\rho_i(\mathbf{r})\}] = \int_V \Big[ \mathcal{F}^{\rm in}_{\rm id}[\{\rho_i(\mathbf{r})\}] + \mathcal{F}^{\rm in}_{\rm exc}[\{\rho_i(\mathbf{r})\}] + \sum_i V_i^{\rm ext}(\mathbf{r}) - \mu_i\, \rho_i(\mathbf{r}) \Big] d\mathbf{r}, \tag{35}$$

where $V_i^{\rm ext}(\mathbf{r})$ represent any external scalar potential acting on species $i \in \{1, ..., \mathrm{n}+\mathrm{m}\}$. For inhomogeneous systems, the (total) ideal free-energy contribution reads

$$\beta\mathcal{F}^{\rm in}_{\rm id}[\{\rho_i(\mathbf{r})\}] = \sum_i \rho_i(\mathbf{r}) \big[ \ln\left(\Lambda_i^3 \rho_i(\mathbf{r})\right) - 1 \big]. \tag{36}$$

The total excess free energy of the system can be decomposed into two contributions, namely,

$$\mathcal{F}^{\rm in}_{\rm exc}[\{\rho_i(\mathbf{r})\}] = \mathcal{F}^{\rm in}_{\rm AOV}[\{\rho_i(\mathbf{r})\}] + \mathcal{F}^{\rm in}_{\rm EMF}[\{\rho_i(\mathbf{r})\}]. \tag{37}$$

The colloid–polymer mixture is now described using the Rosenfeld fundamental-measure framework as extended to the Asakura-Oosawa-Vrij model. This formulation is constructed from the exact zero-dimensional cavity limit of the free energy and therefore satisfies the dimensional crossover condition [20]. Within this framework, the excess free energy of noninteracting polymers can be expressed as

$$\beta\mathcal{F}^{\rm in}_{\rm AOV} = \Phi_1 + \Phi_2 + \Phi_3. \tag{38}$$

The individual terms are defined as

$$\Phi_1 = \sum_{i=1}^{\mathrm{n}+\mathrm{m}} \left[ n_0^i \frac{\partial \phi_0}{\partial n_3^i} \right], \tag{39}$$

$$\Phi_2 = \sum_{i=1,j=1}^{\mathrm{n}+\mathrm{m}} \left( n_1^i n_2^j - \mathbf{n}_{\rm V1}^i \cdot \mathbf{n}_{\rm V2}^j \right) \frac{\partial^2 \phi_0}{\partial n_3^i \partial n_3^j} \tag{40}$$

and

$$\Phi_3 = \frac{1}{8\pi} \sum_{\substack{i=1,j=1 \\ k=1}}^{\mathrm{n}+\mathrm{m}} \left( \frac{n_2^i n_2^j n_2^k}{3} - n_2^i\, \mathbf{n}_{\rm V2}^j \cdot \mathbf{n}_{\rm V2}^k + \frac{3}{2} \left( \mathbf{n}_{\rm V2}^i \mathcal{T}^j \mathbf{n}_{\rm V2}^k - \mathrm{tr}[\mathcal{T}^i \mathcal{T}^j \mathcal{T}^k] \right) \right) \frac{\partial^3 \phi_0}{\partial n_3^i \partial n_3^j \partial n_3^k}, \tag{41}$$

where $\phi_0$ represents the zero-dimensional free energy ($\beta\mathcal{F}_0$) given by $\beta\mathcal{F}_0 = (1 - \sum_{i=\mathrm{n}+1}^{\mathrm{n}+\mathrm{m}} \eta_i - \sum_{j=1}^{\mathrm{n}} \eta_j) \ln(1 - \sum_{i=\mathrm{n}+1}^{\mathrm{n}+\mathrm{m}} \eta_i) - \sum_{i=\mathrm{n}+1}^{\mathrm{n}+\mathrm{m}} \eta_i$. $n_0^i, n_1^i, n_2^i, n_3^i, \mathbf{n}_{\rm V1}^i, \mathbf{n}_{\rm V2}^i$ and $\mathcal{T}$ are the weighted densities, which, for inhomogeneous cases, are given by

$$n_k^i(\mathbf{r}) = \int \omega_k^i(\mathbf{r}' - \mathbf{r}) \rho_i(\mathbf{r}') d\mathbf{r}', \quad k = 0, \ldots, 3, \mathrm{V1}, \mathrm{V2}, \tag{42}$$

where $\omega_k^i$ are weights functions. The the scalar weight functions read

$$\begin{aligned} \omega_0^i(\mathbf{r}) &= \frac{1}{4\pi R_i^2} \delta(\mathbf{r} - R_i), \\ \omega_1^i(\mathbf{r}) &= \frac{1}{4\pi R_i} \delta(\mathbf{r} - R_i), \\ \omega_2^i(\mathbf{r}) &= \delta(\mathbf{r} - R_c), \\ \omega_3^i(\mathbf{r}) &= \Theta(\mathbf{r} - R_c). \end{aligned} \tag{43}$$

Here $R_i$ is the radius of the colloids, i.e., $R_i = \sigma_{ii}/2$, $\Theta(\mathbf{r} - R_i)$ is the Heaviside step function, and $\delta(\mathbf{r} - R_i)$ is the Dirac-delta function. The vector and tensor weight functions are defined as $\omega_{\rm V1}^i(\mathbf{r}) = \omega_1^i(\mathbf{r})\mathbf{r}/r$, $\omega_{\rm V2}^i(\mathbf{r}) = \omega_2^i(\mathbf{r})\mathbf{r}/r$ and $\omega_{\mathcal{T}}^i(\mathbf{r}) = \omega_2^i(\mathbf{r})[\mathbf{r}\mathbf{r}/r^2 - \mathcal{I}/3]$, where $\mathcal{I}$ is the $3 \times 3$ identity matrix. The corresponding weighted densities are obtained in the same way as in Eq. (42), for both colloids and polymers. The details of the methodology and its application are given in the SM [47].

Note that the AOV model, which accounts for the inhomogeneity of the system, provides a good approximation of the depletion effects in colloidal suspensions [20]. In bulk, this formulation reduces to the Rosenfeld formalism for hardcore interactions combined with FV theory, which captures the polymer-induced depletion forces, as discussed earlier.

In the inhomogeneous case, the EMF contribution in $\mathcal{F}^{\rm in}_{\rm exc}$ is given by

$$\beta\mathcal{F}^{\rm in}_{\rm EMF}[\{\rho_i(\mathbf{r})\}] = \frac{1}{2} \sum_{i,j} \rho_i(\mathbf{r}) \int \frac{\rho_j(\mathbf{r}')}{\alpha_j'[\{\rho_c(\mathbf{r}')\}]} \times \phi_{ij}(|\mathbf{r} - \mathbf{r}'|) d\mathbf{r}'. \tag{44}$$

Here, $i, j \in \{1, ..., \mathrm{n}+\mathrm{m}\}$ and $c \in \{\mathrm{n}+1, ..., \mathrm{n}+\mathrm{m}\}$, and $\phi_{ij}$ represents both the polymer-polymer repulsive potential via Eq. (1) and the colloid-polymer attraction. For the latter, instead of using the square well form in Eq. (5), we use a parametrized Gaussian potential, as detailed in the SM [47], which by being continuous provides a better choice for obtaining the numerical solutions of the inhomogeneous densities in one dimension.

The inhomogeneous equilibrium density profile are obtained by minimizing the grand potential $\Omega$ with respect to the densities of the different species, providing the solution [38]

$$\rho_i(\mathbf{r}) = e^{[-V_i^{\rm ext}(\mathbf{r}) + c_i^{(1)}(\mathbf{r}) + \beta\mu_i]}, \tag{45}$$

where $c_i^{(1)}(\mathbf{r}) = -\beta \frac{\partial \mathcal{F}^{\rm in}_{\rm exc}[\{\rho_i\}]}{\partial \rho_i(\mathbf{r})}$, is the one body direct correlation function.

## III. RESULTS FOR A TERNARY MIXTURE WITH TWO POLYMERS AND ONE COLLOIDAL SPECIES

### A. Bulk phase properties

#### *1. Setup and free-energy landscape*

To provide a concrete example of our general approach, we focus on a binary mixture of immiscible polymers, a and b, in which a single colloidal species, c, is dispersed. A well-established realization of this scenario is the polyethylene

glycol–dextran (PEG–dextran) aqueous two-phase system, in which two immiscible polymers of comparable radius of gyration phase-separate while dispersing a third colloidal component commonly at a relatively low concentration. Such systems are widely used in water purification [21] to control the partitioning of different types of pollutants between coexisting phases. Our choice of parameters below reflects this physical setting, allowing us to systematically investigate how polymer size, mutual affinity, and colloid–polymer interactions govern selective partitioning. Here, affinity denotes an effective attractive interaction between polymers and the colloid surface, representing possible electrostatic or hydrophobic interactions. Closely related situations also occur in biological contexts, where phase-separated protein mixtures host additional biomolecular components of similar, but not identical, size. We initially focus on the symmetric case where $R_{aa} = R_{ab} = R_{bb} = \sqrt{2}\sigma$. Without loss of generality, we set $\sigma = 1$ here. The repulsion strength between the polymers are set to correspond to polymers in good solvent, i.e., $\epsilon_{aa} = \epsilon_{bb} = 2.0$ [31], while the cross repulsion parameter is set to $\epsilon_{ab} = 2.5$. This setup fulfills the condition for phase separation at fixed volume, given by [48]

$$\chi = 2\hat{V}_{ab} - [\hat{V}_{aa} + \hat{V}_{bb}] > 0, \tag{46}$$

where $\hat{V}_{ab}$ represents the integrated strength as given in Eq. (23).

For modeling the excluded volume arising from the interaction between polymers and colloids (relevant in $\mathcal{F}_{HC}$ and $\mathcal{F}_{FV}$), we set here $\sigma_{aa} = \sigma_{bb} = \sigma_{cc} = \sigma$. For simplicity, we set some attraction between polymer a and the colloids such that $\hat{V}_{ac} = -2.0$, while the interaction between polymer b and the colloid, as well as the colloid-colloid, are purely repulsive, i.e., $\hat{V}_{cc}, \hat{V}_{bc} = 0$. Note that, in bulk, specifying the values of $\delta$ and $\epsilon_{cp}$ in Eq. (5) is not required due to the integration in Eq. (23) [also expressed analytically in Eq. (24)]. Also, since all sizes are the same here, the only driving force for colloids partitioning rise from their asymmetric attraction with the two polymer species.

We focus on two-phase coexistence, since no stable three-phase coexistence was observed for any of the state points studied in this work, with $\{(\rho_a, \rho_b, \rho_c)^{I}, (\rho_a, \rho_b, \rho_c)^{II}\}$, as in Eq. (28). These densities are obtained by minimizing the free energy defined by Eqs. (6), (7), (9), (11), and (22) under the conditions specified so far. To simplify notation, we will henceforth use $\rho$ to represent the dimensionless form, $\sigma^3\rho$, for all densities. In Fig. 1, we show an example of free energy per particle for the case $\bar{\rho}_a = \bar{\rho}_b = 0.18$ and $\bar{\rho}_c = 0.09$. As expected, the energy landscape exhibits minima at densities corresponding to two distinct coexisting phases in equilibrium. This can be seen in both the $(\rho_a\rho_b)$ plane [Fig. 1(a)] and in the $\rho_b\rho_c$ plane [Fig 1(b)].

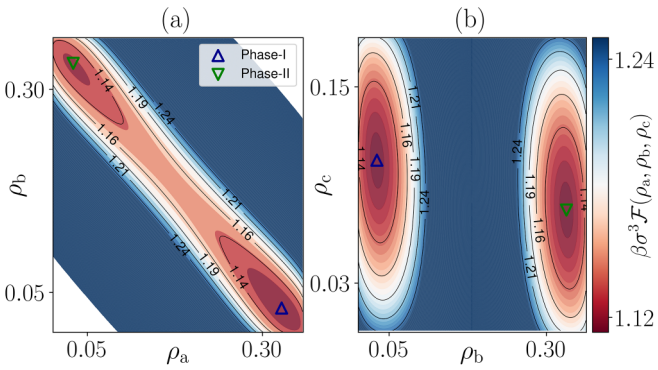


FIG. 1. (a) Free energy per particle, $f$, for a given pair of coexisting densities in the $\rho_a\rho_b$ plane and (b) in the $\rho_b\rho_c$ plane, where a and b are two immiscible polymer species and c a colloidal species. The upper and lower triangles correspond to phase I and phase II, respectively. The color bar indicates the value of $f$ at each point in the density space, where the two conjugate points represent the same system. All conjugate points represent the same grand canonical system consisting of two phases such that $\bar{\rho}_a = \bar{\rho}_b = 0.18$ and $\bar{\rho}_c = 0.09$.

### 2. *Bulk phase response: Comparison with simulations*

Before investigating the effect on phase separation of different physical properties of this ternary system, we provide a comparison between cDFT and particle-based simulations (similar to those in Ref. [[10]). Specifically, we set the polymer-polymer interaction to be Gaussian, as in Eq. (1). For colloid-colloid and colloid-polymer b, we use a standard Lennard-Jones potential cut at its minimum to simulate purely repulsive interactions. For the colloid–polymer interaction with affinity, we employ three different Mie potentials characterized by the exponents u and v. Specifically, we use $48-24$, $24-12$, and $12-6$ potentials. For completeness, the u − v Mie potential is given as

$$\phi_{ac}^{sim}(r) = \frac{u}{u-v}\left(\frac{u}{v}\right)^{v/(u-v)}\epsilon_{ac}\left[\left(\frac{\sigma_{ac}}{r}\right)^{u} - \left(\frac{\sigma_{ac}}{r}\right)^{v}\right]. \tag{47}$$

Potentials analogous to Eq. (47), describing short-ranged interactions between components, are commonly used in coarse-grained models of colloidal systems [49]. Related short-range potentials have also been applied to globular proteins [50], which are frequently represented as hard colloidal particles. This suggests that potentials of this type could provide a more realistic framework than simple hard-sphere models for investigating (bio)molecule partitioning in ATPSs. The parameters used for these interactions are summarized in Table I. The simulations are run in a periodic box with size $15\sigma \times 15\sigma \times 60\sigma$ for a total of $2 \times 10^8$ steps, of which the first half is considered as equilibration time. The dimensionless time step is set to $d\tau = 10^{-4}\sigma^2 D^{-1}$, where $D$ is the particle self-diffusion constant. Equilibration is assessed by observing the individual density profiles until they show no further changes.

Also, in the corresponding cDFT system, polymer-polymer interactions are defined as in Eq. (1), and their parameters as for particle-based simulations (see top part of Table I). When it comes to describing colloid–colloid and colloid–polymer interactions, a one-to-one benchmark is not straightforward. In fact, in our particle-based simulations these interactions are soft, while cDFT considers hard-core repulsion plus eventually attraction. To solve this challenge, we set the size of the corresponding hard-core in cDFT following the Barker-Henderson [51] (BH) perturbation theory. BH theory provides a mapping from a soft repulsive potential to a hard-core

TABLE I. Interactions between all system components in particle-based simulations in bulk.

| Polymer–Polymer - Eq. (1) | | | | |
|---|---|---|---|---|
| | Species | $R_{pq}$ | $\epsilon_{ij}$ | $r_{\text{cutoff}}$ |
| | aa | $\sqrt{2}$ | 2.0 | 3.5 |
| | bb | $\sqrt{2}$ | 2.0 | 3.5 |
| | ab | $\sqrt{2}$ | 2.5 | 3.5 |

| Colloid-Colloid and Colloid–Polymer - Eq. (47) | | | | | |
|---|---|---|---|---|---|
| Species | u | v | $\epsilon_{ij}$ | $\sigma_{ij}$ | $r_{\text{cutoff}}$ |
| cc | 12 | 6 | 1 | 1 | $2^{1/6}$ |
| bc | 12 | 6 | 1 | 1 | $2^{1/6}$ |
| ac (case-I) | 12 | 6 | 0.1757 | 1 | 5 |
| ac (case-II) | 24 | 12 | 0.3104 | 1 | 5 |
| ac (case-III) | 48 | 24 | 0.7565 | 1 | 5 |

diameter, $\sigma_{\text{BH}}$, which is given by

$$\sigma_{ij}^{\text{BH}} = \int_0^{\sigma_{ij}} [1 - e^{-\beta\phi_{ij}(r)}]dr, \tag{48}$$

where $\phi_{ij}$ correspond to the potentials in particle-based simulations with parameters given in the bottom part of Table I. From these interaction potentials and parameters, we obtain $\sigma_{\text{cc}}^{\text{BH}} = \sigma_{\text{bc}}^{\text{BH}} = 0.973$ and $\sigma_{\text{ac}}^{\text{BH}} = 0.874$ for case I, 0.969 for case II, and 1.01 for case III, respectively. We are now left with defining the corresponding attraction strength between polymer a and colloid. To achieve this, we calibrate the value of $\hat{V}_{\text{ac}}$ such that $\Delta\rho_{\text{c}} = \rho_{\text{c}}^{\text{I}} - \rho_{\text{c}}^{\text{II}}$, i.e., the difference in coexisting densities of colloids, in cDFT matches the corresponding particle-based system. We do this under the following conditions: $\bar{\rho}_{\text{a}} = \bar{\rho}_{\text{b}} = 0.27$, $\bar{\rho}_{\text{c}} = 0.09$. For case I (see Table I), we find a good match for $\hat{V}_{\text{ac}} = -3.0$, while for case II $\hat{V}_{\text{ac}} = -2.8$, and for case III $\hat{V}_{\text{ac}} = -2.5$.

To show the validity of the cDFT predictions on the phase response of the system, in Fig. 2(a) we vary the total polymer density, $\bar{\rho}_{\text{p}}$, from 0.54 to 0.8 with $\bar{\rho}_{\text{a}} = \bar{\rho}_{\text{b}}$, while keeping $\bar{\rho}_{\text{c}}$ fixed at 0.09. The predictions of our cDFT are benchmarked against particle-based simulations for all three cases. Figure 2(a) shows a monotonic increase in partitioning of the colloids as the total polymer density is increased. We also see that our improved MF approach performs better in all cases up to high colloidal density. Similarly, in Fig. 2(b), we vary the density of the colloids from $\bar{\rho}_{\text{c}} = 0.09$ to 0.4 while keeping $\bar{\rho}_{\text{a}} = \bar{\rho}_{\text{b}} = 0.27$ fixed. Interestingly, we see a decrease in partitioning after reaching a maximum value at around $\bar{\rho}_{\text{c}} = 0.2$. The presence of colloids increases the effective polymer density by reducing the available volume, which in turn lowers the free energy through enhanced polymer–colloid attraction. This effect, however, reaches a maximum, as the gain is compensated by increased colloid–colloid and polymer–polymer repulsive interactions, along with a further reduction in available volume that limits polymer–colloid contributions when colloids are too close to each other. Also, here the cDFT predictions are in good agreement with simulations, up to high colloidal concentrations. We can see that, with the exception of case I, the EMF approach performs better than its standard version.

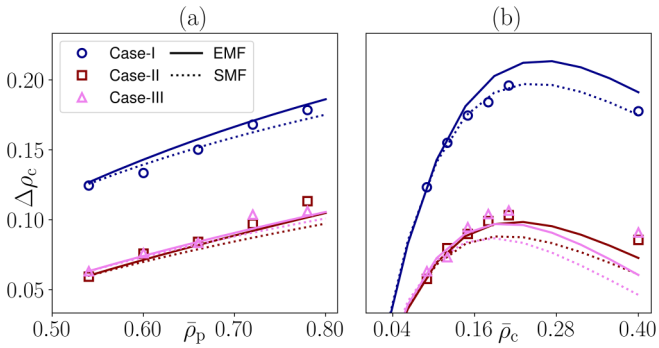


FIG. 2. Density difference between the two phases of the colloidal species $\Delta\rho_{\text{c}} = \rho_{\text{c}}^{\text{I}} - \rho_{\text{c}}^{\text{II}}$ are shown using symbols for particle-based Brownian dynamics simulations (similar to those in [10]). The simulation results for the parameters summarized in Table I are shown for cases I–III and are compared with our cDFT using EMF (solid lines), as well as SMF (dashed lines). (a) Results while varying the total polymer concentration ($\bar{\rho}_{\text{p}} = \bar{\rho}_{\text{a}} + \bar{\rho}_{b}$) at fixed colloid concentration $\bar{\rho}_{\text{c}} = 0.09$. (b) Results for varying colloid density at fixed polymer concentration $\bar{\rho}_{\text{a}} = \bar{\rho}_{\text{b}} = 0.27$.

To investigate this specific case, the sensitivity of both MF approaches with respect to the value of $\sigma_{\text{BH}}$ has been addressed. We find that the EMF approach remains more anchored to the presented predictions, while the SMF approach deviates from the presented curve quite rapidly. All in all, the present EMF implementation yields improved agreement with simulation results compared to the standard MF treatment.

#### *3. Effect of polymer properties on the phase response*

To further explore the effect of polymer properties on the phase response of the ternary mixture, we calculate the coexisting densities for a system at different total polymer concentration $\bar{\rho}_{\text{p}} = \bar{\rho}_{a} + \bar{\rho}_{b}$. We explore $\bar{\rho}_{\text{p}}$ ranging between 0.23 and 1.1 at fixed average colloid concentration $\bar{\rho}_{\text{c}} = 0.09$. Here the parameters are as follow: $R_{\text{aa}} = R_{\text{bb}} = R_{\text{ab}} = \sqrt{2}\sigma$, $\epsilon_{\text{aa}} = \epsilon_{\text{bb}} = 2.0$, $\epsilon_{\text{ab}} = 2.5$, $\sigma_{\text{aa}} = \sigma_{\text{bb}} = \sigma_{\text{cc}} = \sigma$, and $\hat{V}_{\text{ac}} = -5.6$. The phase response is shown in the $x - y$ plane in Fig. 3(a), where $x, y$ are the reduced densities such that $\rho_{\text{a}} = (1-x)(1-y)\rho_{\text{t}}$, $\rho_{\text{b}} = x(1-y)\rho_{\text{t}}$, and $\rho_{\text{c}} = y\rho_{\text{t}}$. Note that $x$ corresponds to the relative concentration of polymer b with respect to the total amount of polymers, while $(1-x)$ the relative concentration of polymer a. $y$ represents the fraction of colloids relative to the total number of system components, including both polymer species and colloids. In Fig. 3(b), we show the coexisting colloidal densities as a function of $x$. The coexisting phases are shown by upper and lower triangles, respectively, and are connected by tie lines (isobars). The color of the tie lines corresponds to the total density of the polymers, $\bar{\rho}_{\text{p}}$, for which $\bar{\rho}_{a} = \bar{\rho}_{b}$. The critical point, denoted by the full circle, is found at $\bar{\rho}_{\text{a}} = \bar{\rho}_{b} = 0.1125$ and $\bar{\rho}_{\text{c}} = 0.09$. This is slightly smaller than the value obtained by considering only the presence of polymers, which we find to be $\bar{\rho}_{\text{a}} = \bar{\rho}_{b} = 0.135$. This clearly underlines the effect of the colloidal species in the phase separation of polymers, although being at a relative low concentration. We also see that as $\bar{\rho}_{\text{p}}$ is increased, the colloids partition more strongly within phase

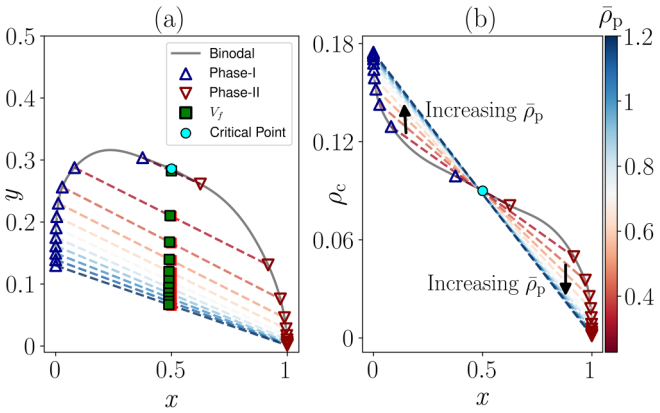


FIG. 3. In (a), binodal curve for the ternary colloid-polymer mixture described by the following parameters: $R_{aa} = R_{bb} = R_{ab} = \sqrt{2}\sigma$, $\epsilon_{aa} = \epsilon_{bb} = 2.0, \epsilon_{ab} = 2.5$, $\sigma_{aa} = \sigma_{bb} = \sigma_{cc} = 1$, and $\hat{V}_{ac} = -5.6$. $x$ is the fraction of polymer b with reference to the total polymer densities $\bar{\rho}_p$ and $y$ is the fraction of colloids with reference to the total density $\bar{\rho}_t$. Here $\bar{\rho}_c = 0.09$ is kept fixed. The upper triangles indicate phase I (polymer a-rich phase), while the lower triangles indicate phase II (polymer b-rich phase). Coexisting points are connected by isobars, where their color corresponds to the value of $\bar{\rho}_p$. The green squares represent the value of $V_f$, i.e., the volume ratio of phase I, while the red squares represent $V_f = 0.5$. The full circle represents the critical point. In (b), effect of polymer concentration on the coexistence densities of colloids.

I. This is expected, as the colloids favor the polymers making up said phase.

For the same system configuration, we vary the affinity between polymer a and colloids via $\hat{V}_{ac}$. In Fig. 4, we show the coexisting densities of the colloids in the two phases for $\hat{V}_{ac} = -2.8$ [Fig. 4(a)], $\hat{V}_{ac} = -5.6$ [Fig. 4(b)]), and $\hat{V}_{ac} = -8.4$ [Fig. 4(c)]. As expected, as $\hat{V}_{ac}$ is increased, colloids accumulate progressively within phase I. In line with the finding in Fig. 3(b), this effect is more pronounced as the total polymer density is increased. We also find a small deviation of the coexistence points from $x = 0.5$ to smaller values of $x$ as $\hat{V}_{ac}$

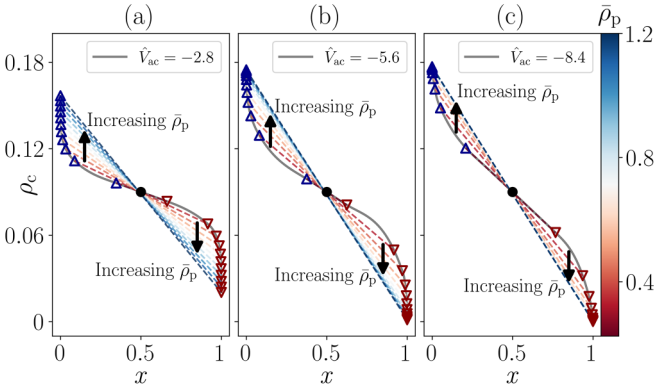


FIG. 4. Partitioning of colloids driven for the same system as in Fig. 3 yet for (a) $\hat{V}_{ac} = -2.8$, (b) $\hat{V}_{ac} = -5.6$, and (c) $\hat{V}_{ac} = -8.4$. The upper triangles indicate phase I (polymer a-rich phase), while the lower triangles indicate phase II (polymer b-rich phase). Coexisting points are connected by isobars, where their color corresponds to the value of $\bar{\rho}_p$.

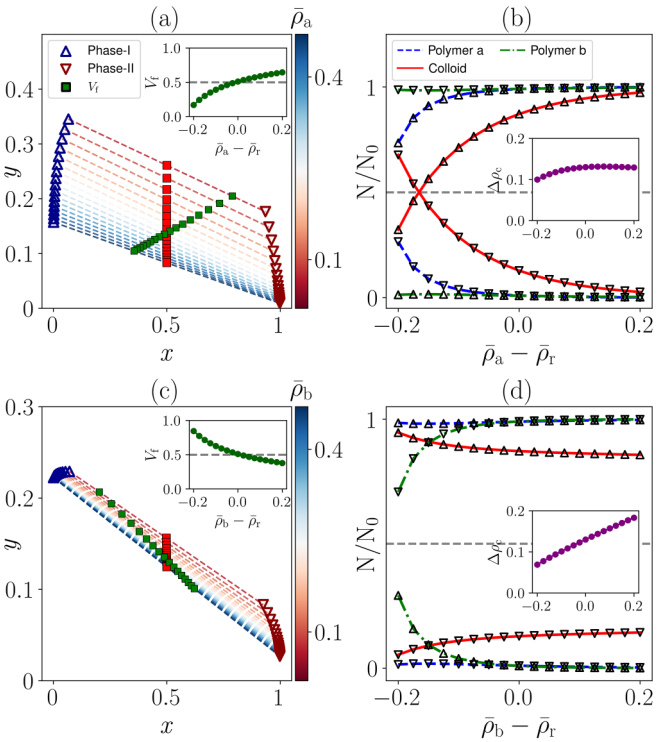


FIG. 5. System interacting as in Fig. 3. Here $\rho_r = 0.27$ and $\bar{\rho}_c = 0.09$ are fixed. (a) Phase response. (b) Partitioning of the system components for varying $\bar{\rho}_a$. (c) Phase response (d) Partitioning of the system components for varying $\bar{\rho}_b$. Upper triangles indicate phase I (polymer a-rich phase), while lower triangles indicate phase II (polymer b-rich phase). Coexisting points are connected by isobars, where their color corresponds to the value of $\bar{\rho}_a$ [(a)] and $\bar{\rho}_b$ [(c)]. The green squares represent the value of $V_f$, i.e., the volume ratio of phase I, while red squares represent $V_f = 0.5$. The differences in the coexisting densities of the colloids, $\Delta\rho_c$, are shown in the insets of (b) and (d). Dashed horizontal lines shown in (b) and (d) represent $N/N_0 = 0.5$.

is increased, indicating a small enhancement in the polymer phase separation driven by the presence of the colloids. This is in line with previous findings [10].

So far, we focused on the symmetric case $\bar{\rho}_a = \bar{\rho}_b$. To investigate the effect of the relative amount of the two polymer species, we now fix the colloids density $\bar{\rho}_c = 0.09$ and one polymer species in turn. The results are shown in Fig. 5, which illustrates a simple case of composition-driven phase separation, similar to those that can be observed in biological systems, such as, e.g., protein solutions (see, e.g., [52]). Specifically, in Figs. 5(a) and 5(b), we fix $\bar{\rho}_b = \rho_r = 0.27$ and vary $\bar{\rho}_a$ around the reference value, $\rho_r$. As one can see in Fig. 5(a), the difference between the coexisting densities of the colloids in the two phases remain almost unaltered (the tielines are practically parallel). This can also be seen in the inset of Fig. 5(b), where $\Delta\rho_c$ changes, and correlates with the value of $\bar{\rho}_a$. The coexisting densities of the polymers, however, depends on $\bar{\rho}_a$, as expected. To compensate the change in the density of species a, a shift in $V_f$ away from value of the symmetric case, $V_f = 0.5$, is observed [see also inset of Fig. 5(a)]. Figure 5(b) shows the variation in the number of particles, normalized by their total amount in the

system, $N_0$, of the different system components as a function of $\bar{\rho}_a$ in the two phases. When $\bar{\rho}_\mathrm{a}$ is small, polymer a barely phase separate, yet partitioning is quickly increased as $\bar{\rho}_a$ is increased. Interestingly, there is a crossover of the partitioning of the colloids. In fact, for small values of $\bar{\rho}_a$, colloids prefer phase II. This trend is then reversed as $\bar{\rho}_a$ is increased. The partitioning of the colloids correlates with an increased volume of phase I. Nevertheless, as already mention above, the coexisting densities of the colloids in the two phases vary only marginally [see inset of Fig. 5(b)] and the relative amount of polymer b in the two phases is practically unaffected.

Figures 5(c) and 5(d) show the effect of varying $\bar{\rho}_\mathrm{b}$ while keeping $\bar{\rho}_\mathrm{a} = \rho_\mathrm{r} = 0.27$ and $\bar{\rho}_\mathrm{c}$ constant. Also, here we see a strong dependency of the relative volume of the two phases (through the value of $V_\mathrm{f}$) as a function of $\bar{\rho}_\mathrm{b}$. As expected for these conditions, the volume of phase II increases with $\bar{\rho}_\mathrm{b}$. This is shown in Fig. 5(c) and its inset. This, in turn, is expected to have an effect on the partitioning of the colloids. When considering the number of colloids in the different phases, the change seems marginal, as shown in Fig. 5(d). However, when it comes to the difference between the coexisting densities of the colloids, $\Delta\rho_c$ [see inset of Fig. 5(d)], the effect is relatively important. Similar to Figs. 5(a) and 5(b), we observe the same trends in the partitioning of the two polymer species. Next, we address the effect of polymer species densities by maintaining the occupied volume fractions fixed. This variation corresponds to a case in which the polymerization (or length of the polymers) is controlled. The interactions between the system components are the same as above, with the exception of $R_{ij}$, which will change according to Eq. (2). Note that as $R_{ij}$ is changed, also the value of $\sigma_{ij}$ has to change accordingly. Specifically, $\sigma_{ii} = \sigma R_{ii}/R_\mathrm{r}$ for $i = \mathrm{a}, \mathrm{b}$, where $R_\mathrm{r} = \sqrt{2}\sigma$. First, we set $\varphi_\mathrm{a} = \frac{4}{3}\pi R_{\mathrm{aa}}^3 \bar{\rho}_\mathrm{a} = 3.2$ and $\varphi_\mathrm{b} = \frac{4}{3}\pi R_{\mathrm{bb}}^3 \bar{\rho}_\mathrm{b} = 3.2$, yet allowing both $R_{\mathrm{aa}}$ and $\bar{\rho}_\mathrm{a}$ to vary. Figure 6(a) shows the change in coexistence densities for different values of $\bar{\rho}_\mathrm{a}$ with respect to the reference density $\rho_\mathrm{r} = 0.27$. The coexisting densities of the polymers do not show a strong dependency on $\bar{\rho}_\mathrm{a}$, yet the value of $V_\mathrm{f}$ increases importantly with the latter. The polymer partitioning also remains practically unchanged, as can be seen in Fig. 6(b). This behavior is not observed in Fig. 5(b), where the partitioning of polymer a is strongly influenced by its density. The distribution of colloids is similarly affected by the increase in $\bar{\rho}_\mathrm{a}$, which corresponds to a decrease in $\sigma_{\mathrm{aa}}$. This is true both in terms of particle distribution [Fig. 6(a)], as well as in terms of coexisting densities [inset of Fig. 6(b)]. Second, we set $\varphi_\mathrm{a} = \frac{4}{3}\pi R_{\mathrm{aa}}^3 \bar{\rho}_\mathrm{a} = 3.2$ and $\varphi_\mathrm{b} = \frac{4}{3}\pi R_{\mathrm{bb}}^3 \bar{\rho}_\mathrm{b} = 3.2$, yet allowing both $R_{\mathrm{bb}}$ and $\bar{\rho}_\mathrm{b}$ to vary. Also here, the effect on polymer coexistence is marginal, however, the change of corresponding volume of the two phases is important [see Fig. 6(c)]. Similar to panel (b), also the partitioning of the polymers is marginally affected by the value of $\bar{\rho}_\mathrm{b}$. In contrast to Fig. 5(d), where polymer b partitioning increases with $\bar{\rho}_\mathrm{b}$, the colloid partitioning weakens while $\Delta\rho_\mathrm{c}$ grows. Finally, to explore the effect of asymmetry in polymer sizes, corresponding to asymmetry in depletion forces, we change the size of one polymer species while fixing the size of the other. Such variation is relevant, as it has been recently shown experimentally that systems containing mostly short polymers exhibit a narrower two-phase

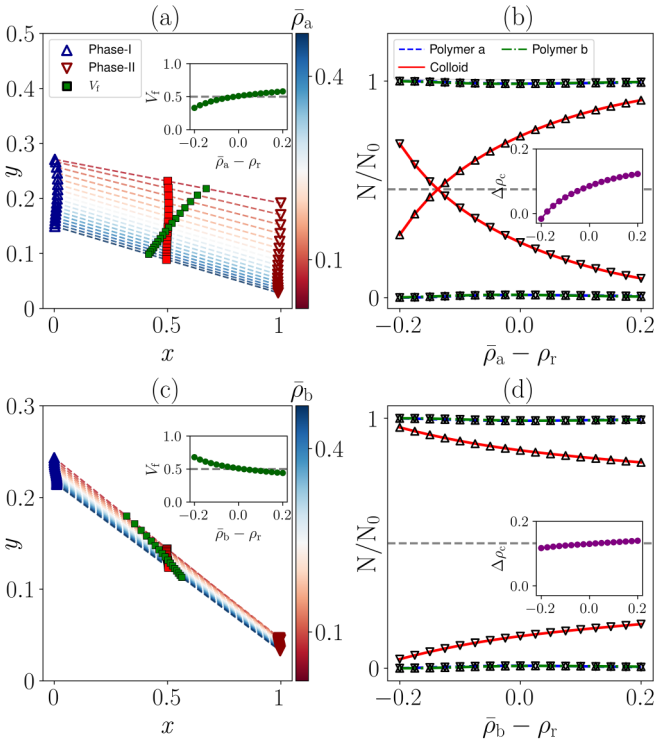


FIG. 6. System interacting as in Fig. 3 with the exception of $R_{ij}$ following Eq. (2). Here $\rho_\mathrm{r} = 0.27$ and $\bar{\rho}_\mathrm{c} = 0.09$ are fixed. (a) Phase response. (b) Partitioning of the system components for varying $\bar{\rho}_\mathrm{a}$ under the constraint $\varphi_\mathrm{a} = \frac{4}{3}\pi R_{\mathrm{aa}}^3 \bar{\rho}_\mathrm{a} = 3.2$ and $\varphi_\mathrm{b} = \frac{4}{3}\pi R_{\mathrm{bb}}^3 \bar{\rho}_\mathrm{b} = 3.2$ with varying $R_{\mathrm{aa}}$. (c) Phase response (d) Partitioning of the system components for varying $\bar{\rho}_\mathrm{b}$ under the constraint $\varphi_\mathrm{a} = \frac{4}{3}\pi R_{\mathrm{aa}}^3 \bar{\rho}_\mathrm{a} = 3.2$ and $\varphi_\mathrm{b} = \frac{4}{3}\pi R_{\mathrm{bb}}^3 \bar{\rho}_\mathrm{b} = 3.2$ with varying $R_{\mathrm{bb}}$. Note that $\sigma_{\mathrm{bb}} = \sigma R_{\mathrm{bb}}/R_\mathrm{r}$, where $R_\mathrm{r} = \sqrt{2}\sigma$. The upper triangles indicate phase I (polymer a-rich phase), while the lower triangles indicate phase II (polymer b-rich phase). Coexisting points are connected by isobars, where their color corresponds to the value of $\bar{\rho}_\mathrm{a}$ [(a)] and $\bar{\rho}_\mathrm{b}$ [(c)]. The green squares represent the value of $V_\mathrm{f}$, i.e., the volume ratio of phase I, while the red squares represent $V_\mathrm{f} = 0.5$. The differences in the coexisting densities of the colloids, $\Delta\rho_\mathrm{c}$, are shown in the insets of (b) and (d). Dashed horizontal lines shown in (b) and (d) represent $N/N_0 = 0.5$.

region, together with a reduced density differences [53]. Also, here we keep the average densities fixed ($\bar{\rho}_\mathrm{a} = \bar{\rho}_\mathrm{b} = 0.27$ and $\bar{\rho}_\mathrm{c} = 0.09$) and the interaction strength between colloids and polymer a at $\hat{V}_{\mathrm{ac}} = -5.6$. With $R_\mathrm{r} = \sqrt{2}\sigma$ being the reference polymer size, in Figs. 7(a) and 7(b), we investigate the effect of $R_{\mathrm{aa}}$ on phase separation and partitioning, respectively, while keeping $R_{\mathrm{bb}} = R_\mathrm{r}$. Note that any change in polymer size implies a change in the value of $\sigma_{ii}$, which is linearly rescaled correspondingly, i.e., $\sigma_{ii} = \sigma R_{ii}/R_\mathrm{r}$, where $i = \mathrm{a}, \mathrm{b}$. In Fig. 7(a), we see that the coexisting densities of the polymers are practically unaffected by the value of $R_{\mathrm{aa}}$, while the phase boundary, described by $V_\mathrm{f}$, shifts. Specifically, when $R_{\mathrm{aa}} > R_\mathrm{r}$, phase I (polymer a-rich phase) increases in volume. Nevertheless, the partitioning of each species [shown in Fig. 7(b)], remain practically unaffected, with a slight variation for small values of $R_{\mathrm{aa}}$ in $N/N_0$ for polymer a. However, this small change points toward a narrowing of the phase separation region of the polymer mixture, in line with Ref. [[53]. The

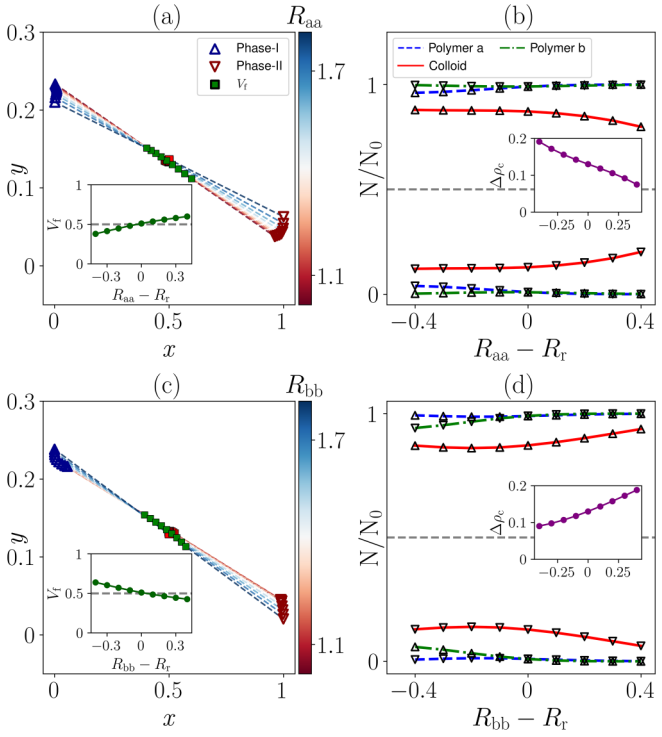


FIG. 7. Here $\bar{\rho}_a = \bar{\rho}_b = 0.27$ and $\bar{\rho}_c = 0.09$ with $\hat{V}_{ac} = -5.6$. Coexistence densities (a) and partitioning (b) of system components for varying sizes of polymer a, where $R_{bb} = \sqrt{2}\sigma = R_r$. Note that $R_{ab}$ follows from Eq. (2). Coexistence densities (c) and partitioning (d) of system components for varying sizes of polymer b, where $R_{aa} = \sqrt{2}\sigma = R_r$. The upper triangles indicate phase I (polymer a-rich phase), while the lower triangles indicate phase II (polymer b-rich phase). Coexisting points are connected by isobars, where their color corresponds to the value of $R_{aa}$ and $R_{bb}$ in (a) and (c), respectively. The green squares represent the value of $V_f$, i.e., the volume ratio of phase I, while the red squares represent $V_f = 0.5$. Full circle represents the critical point. Dashed horizontal lines shown in (b) and (d) represent $N/N_0 = 0.5$.

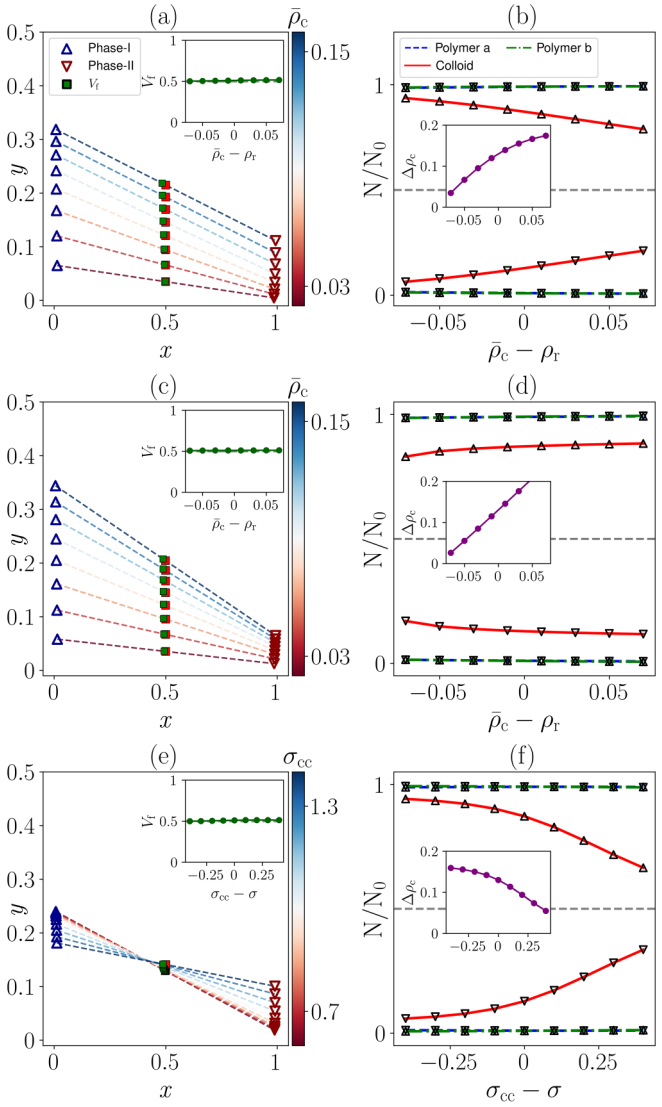


FIG. 8. Here $R_{aa} = R_{bb} = R_{ab} = \sqrt{2}\sigma$, $\epsilon_{aa} = \epsilon_{bb} = 2.0$, $\epsilon_{ab} = 2.5$, $\sigma_{aa} = \sigma_{bb} = \sigma$, and $\hat{V}_{ac} = -5.6$. Additional constraints include $\bar{\rho}_a = \bar{\rho}_b = 0.27$ and reference density $\rho_r = 0.09$. (a) Phase response. (b) Partitioning of the system components for varying $\bar{\rho}_c$. (c) Phase response. (d) Partitioning of the system components for varying $\bar{\rho}_c$ with fix volume fraction $\varphi_c = \frac{4}{3}\pi(\sigma_{cc}/2)^3\bar{\rho}_c = 0.04712$, with $\bar{\rho}_c = 0.09$ ($\sigma_{cc}$ varies accordingly). (e) Phase response. (f) Partitioning of the different system components for $\bar{\rho}_c = 0.09$ for varying colloids size, $\sigma_{cc}$. The upper triangles indicate phase I (polymer a-rich phase), while the lower triangles indicate phase II (polymer b-rich phase). Coexisting points are connected by isobars (see color bar). The green squares represent the value of $V_f$, while the red squares represent $V_f = 0.5$. The differences in the coexisting densities of the colloids, $\Delta\rho_c$ shown in the insets of (b), (d), and (f). Dashed horizontal lines shown in (b), (d), and (f) represent $N/N_0 = 0.5$.

difference in coexisting densities of the colloids decreases importantly as $R_{aa}$ is increased. Similarly, in Figs. 7(c) and 7(d), we study the same response yet as a function of $R_{bb}$. Also in this case, as shown in Fig. 7(c), the values of the coexisting densities are barely affected, yet the phase boundary shifts such that the volume of phase II increases as $R_{bb}$ is increased. Also, similar to the previous case, the partitioning of the different system components are practically unchanged [Fig. 7(d)]. Conversely, the inset of Fig. 7(d) shows that the difference of coexisting densities of the colloids correlates with the size of polymer b.

#### *4. Effect of colloids properties on the phase response*

To examine the effect of physical properties of the colloidal species on the system phase response and partitioning, we investigate the effects of colloid density and relative sizes. Besides the variations specified hereafter, the interactions describing the system are $R_{aa} = R_{bb} = R_{ab} = \sqrt{2}\sigma$, $\epsilon_{aa} = \epsilon_{bb} = 2.0$, $\epsilon_{ab} = 2.5$, $\sigma_{aa} = \sigma_{bb} = \sigma$, and $\hat{V}_{ac} = -5.6$. For all cases addressed here, the polymer densities are fixed to $\bar{\rho}_a = \bar{\rho}_b = 0.27$. Here we define the reference colloidal density, $\rho_r = 0.09$. Specifically, in Figs. 8(a) and 8(b) we investigate the effect of $\bar{\rho}_c$ on the phase response and partitioning, respectively, of colloids with size $\sigma_{cc} = \sigma_{aa} = \sigma_{bb} = \sigma$. From both Figs. 8(a) and 8(b), we can see that the amount of colloids has a marginal effect on the coexisting densities of the polymers (almost no variation in the value of $x$, and the change in $y$ is

compensated by the same change in $\rho_t$), as well as a marginal influence on $V_f$. However, the difference in coexisting densities of the colloids clearly increases as shown in the inset of Fig. 8(b). In contrast, partitioning of the colloids between the two phases decreases with increasing $\bar{\rho}_c$, as the finite volume of polymers limits their ability to attract colloids in the same proportion [red curve in Fig. 8(b)}. In Figs. 8(c) and 8(d), we address the effect of colloidal density, under the constraint of constant occupied volume fraction, which is achieved by changing $\sigma_{cc}$ accordingly, as the volume fraction of the colloids is given by $\varphi_c = \frac{4}{3}\pi(\sigma_{cc}/2)^3\bar{\rho}_c$. Here, $\varphi_c = 0.04712$. We find that changing the colloid density while keeping the packing fraction constant does not significantly alter the polymer phase behavior [Fig. 8(c)]. However, colloid partitioning increases when a larger number of smaller colloids are present (higher values of $\bar{\rho}_c$), as shown in Fig. 8(d). This is opposite to the trend in Fig. 8(b), highlighting the role of colloid size in partitioning, despite both polymer species exerting the same depletion force ($\sigma_{aa} = \sigma_{bb}$). Finally, in Figs. 8(e) and 8(f), for fixed $\bar{\rho}_c$, we vary the size of the colloids, $\sigma_{cc}$, around the reference value, $\sigma$. Also here, as shown in Figs. 8(c) and 8(d), the effect on polymer coexistence is marginal (same for $V_f$). Instead, colloid size has a strong impact on colloid partitioning itself. As the colloid size decreases, partitioning increases [Fig. 8(f)], even if the colloids exert the same depletion force on both the polymers ($\sigma_{aa} = \sigma_{bb}$). This is due to a shift in the competition between depletion forces and attractive forces, which makes attractive forces more dominant for smaller colloids. This last results underlines the importance of polymer-colloid size ratio in controlling partitioning.

### B. Inhomogeneous properties

We conclude by examining the inhomogeneous density profiles of the system for a specific case. In addition to providing a typical response, we also compare our cDFT results with particle-based simulations. To this end, we confine the mixture between two parallel walls perpendicular to the $z$ axis, described by the potential

$$u_w(z) = \epsilon\left(\frac{2}{15}\left(\frac{\sigma}{z}\right)^9 - \left(\frac{\sigma}{z}\right)^3\right), \tag{49}$$

where $z$ is the distance from the wall. We start by defining the interactions and the thermodynamic state point for particle-based simulations. Here the polymer-polymer interactions are modeled using $R_{aa} = R_{bb} = R_{ab} = \sqrt{2}\sigma$, $\epsilon_{aa} = \epsilon_{bb} = 2.0$, and $\epsilon_{ab} = 2.5$. The colloid-colloid and colloid-polymer interactions follow Eq. (47), with the parameters specified in Table II. The simulations are run in a box with size $15\sigma \times 15\sigma \times 60\sigma$ for a total of $2 \times 10^8$ steps, of which the first half is considered as equilibration time. Also here, $d\tau = 10^{-4}\sigma^2 D^{-1}$, where $D$ is the particle self-diffusion constant.

Also here, the colloid has an affinity with polymer a, while colloid-colloid and colloid-polymer b interactions are purely repulsive. We focus on the following densities: $\bar{\rho}_a = 0.27$, $\bar{\rho}_b = 0.27$, and $\bar{\rho}_c = 0.09$. The particle-based simulations results are obtained by means of standard Brownian dynamics simulations, as in [10]. The simulations are run in a box with size $15\sigma \times 15\sigma \times 60\sigma$ for a total of $2 \times 10^8$ steps, of which the first half is considered as equilibration time. Also here, the dimensionless time step is set to $d\tau = 10^{-4}\sigma^2 D^{-1}$. Equilibration is evaluated by monitoring the individual density profiles until they remain unchanged.

TABLE II. Colloid-colloid and colloid–polymer interaction parameters for the inhomogeneous system in particle-based simulations.

| Colloid-colloid and colloid–polymer | | | | | |
|---|---|---|---|---|---|
| Species | u | v | $\epsilon_{ij}$ | $\sigma_{ij}$ | $r_{cutoff}$ |
| cc | 12 | 6 | 1 | 1 | $2^{1/6}$ |
| bc | 12 | 6 | 1 | 1 | $2^{1/6}$ |
| ac | 36 | 18 | 1.6358 | 1 | 5 |

Finding the corresponding cDFT profiles requires two main steps. In the first step, one has to solve for bulk coexistence by specifying the average densities, $\bar{\rho}_a$, $\bar{\rho}_b$, and $\bar{\rho}_c$. The polymers can be mapped directly from the simulations, while colloid-colloid and colloid-polymer interactions require the calculation of effective sizes, which is done using Eq. (48). The corresponding BH diameter for this specific system are $\sigma_{cc}^{BH} = \sigma_{bc}^{BH} = 0.989$ and $\sigma_{ac}^{BH} = 0.986$. Again, the contribution from the attractive interactions within the MF approximation is not uniquely defined. To overcome this issue, we vary the value of $\hat{V}_{ac}$ in cDFT to match the coexisting colloidal densities [54]. We find the best fit for $\hat{V}_{ac} = -9.132$. We can now carry out the second step, which consists of solving the inhomogeneous cDFT with the initial guesses obtained in bulk [55]. This is done by solving Eq. (45) iteratively, with the chemical potentials obtained in bulk. The evaluation of $\mathcal{F}_{exc}[\{\rho_i(z)\}]$ requires integration over the $x$ and $y$ axes for the free-energy functionals described in Sec. II C.

We use a Picard iteration, namely,

$$\rho_i^k(z) = \alpha\rho_i^{new}(z) + (1-\alpha)\rho_i^{k-1}(z), \tag{50}$$

where $k$ is the iteration step and $\alpha$ is a mixing parameter. We employ $\alpha = 0.001$ for $\bar{\rho}_c < 0.12$ and $\alpha = 10^{-5}$ for $\bar{\rho}_c \geqslant 0.12$. Further details, including the numerical implementation, are provided in the SM [47].

The density profiles for this specific case are shown in Fig. 9. We find a satisfactory matching between the particle-based simulations and our cDFT. Most satisfactory is the matching of the coexisting densities, including both polymer and colloidal species, together with the first density peaks at the walls. However, the position and shape of the interface between the two phases is captures only qualitatively. Specifically, the interface is sharper in cDFT and shows additional undulations which are inexistent in the particle-based simulations, as previously observed [56]. These undulations are known to be exaggerated by the MF approximation [57]. Nevertheless, although the system is highly complex and the simulations rely on soft potentials while cDFT assumes hard interactions, the theory provides very valuable physical insight.

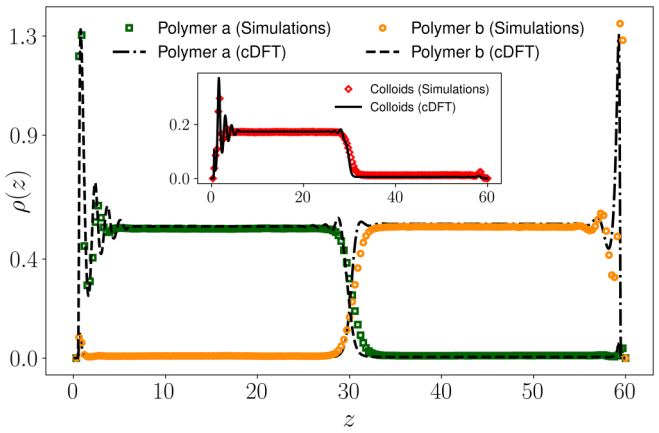


FIG. 9. Density profiles for a ternary colloid–polymer mixture. Polymer-polymer interactions are modeled using $R_{aa} = R_{bb} = R_{ab} = \sqrt{2}\sigma$ and $\epsilon_{aa} = \epsilon_{bb} = 2.0$, $\epsilon_{ab} = 2.5$. Colloid-colloid and colloid-polymer interactions follow Eq. (47), with the parameters specified in Table II. Average densities are $\bar{\rho}_a = 0.27$, $\bar{\rho}_b = 0.27$, and $\bar{\rho}_c = 0.09$. Confinement is imposed with Eq. (49). Solid lines denote cDFT predictions, while dashed lines correspond to particle-based Brownian dynamics simulations (as in [10]).

## IV. CONCLUSIONS AND PERSPECTIVE

In this work, we proposed a general scheme for studying the bulk multiphase coexistence for a mixture composed by n polymer and m colloidal species with different affinities. This scheme can be applied to bimolecular condensates [25], where several polymeric fluid phases coexist with other dispersed macromolecules. In the scheme, we proposed an enhanced mean field approach within the classical density functional theory formalism [11]. For the case of two demixing polymer species and one dispersed colloidal component affine to only one polymer type, our scheme has been benchmarked with particle-based simulations. We found both qualitative and quantitative results (see Figs. 2 and 9). This specific case is relevant in the context of water purification by means of aqueous two-phase systems [21,22], involving demixing of similarly sized incompatible polymers and asymmetric partitioning of an additional dilute component between the two phases. We found that the partitioning of the colloidal species is strongly influenced by its affinity for the affine polymer and by the polymer's density (higher density leads to stronger partitioning), as well as by the polymer–colloid size ratio (smaller colloids partition more readily), whereas changes in the density of the non-affine polymer and polymer size asymmetry have only a weak effect on colloid partitioning.

Notably, our findings resonate with previous studies on colloidal systems in binary solvent mixtures near their critical point [58,59], which also reported rich phase behavior and highlighted the role of parameters such as colloid size, colloid wettability, and distance from the critical point, in controlling phase behavior. Although the physical systems are quite different (binary solvents in their case and immiscible polymers in water in ours), the parallels highlight the broader relevance of these mechanisms across several soft matter systems. Another interesting case that shares similarities with our work is the recent study of ouzo [46], which consists of a ternary mixture of water, alcohol and trans-anethole oil. In this work, the experimental bulk phase diagram and interfacial properties have been benchmarked against a lattice DFT approach.

From an experimental perspective, in the case of soluble yet demixing polymers, it is safe to assume $\epsilon_{aa} = \epsilon_{bb} = 2k_BT$ [31], while the value of $\epsilon_{ab}$ should be fitted from experiments at different polymer concentrations. Similarly, the affinity between the polymer species and the colloids can be inferred from experimental measurements of the second virial coefficients, e.g., via static light scattering [60].

It is important to note that the current formalism is valid only for additive mixtures of spherical, charge-neutral constituents. Nevertheless, density functional theory approaches that address this gap have already been developed (see, e.g., [61–63]). We hope that future work will integrate such advances into our formalism, as extending our scheme to include these features, while challenging, remains feasible.

## ACKNOWLEDGMENTS

This work was supported by the Jane ja Aatos Erkon Säätiö under Grant No. 230052 (A.S.). Computational resources by CSC IT Center for Finland are also gratefully acknowledged. The work was conducted within the #SUSMAT profiling measure at the University of Turku, Finland. We are also thankful to Prof. A. Archer for fruitful discussions.

V.A.V. carried out the work under the supervision of A.S. and wrote the first draft of the manuscript. A.S. conceived the idea and secured the funding for the work. All authors contributed to writing and reviewing.

## DATA AVAILABILITY

Link to the developed algorithms and open data is provided at [64] . If using the algorithms or the open data, we request acknowledging the authors by citing the original source (this paper).

[1] A. A. Hyman, C. A. Weber, and F. Jülicher, Liquid-liquid phase separation in biology, Annu. Rev. Cell Dev. Biol. **30**, 39 (2014).

[2] M. Balakrishnan and A. K. Kenworthy, Lipid peroxidation drives liquid–liquid phase separation and disrupts raft protein partitioning in biological membranes, J. Am. Chem. Soc. **146**, 1374 (2024).

[3] D. Mejías, V. Seballos, and L. Lafon-Hughes, Liquid–liquid phase separation and poly (ADP–ribosyl)ation in the context of ultraviolet radiation-induced stress in mammalian cells, Biophys. Rev. **17**, 499 (2025).

[4] Y. Shin and C. P. Brangwynne, Liquid phase condensation in cell physiology and disease, Science **357**, eaaf4382 (2017).

[5] T. K. Georgiou, R. Hoogenboom, and A. Kikuchi, Introduction to trends in thermoresponsive polymers: From chemistry to applications, Polym. Chem. **16**, 233 (2025).

[6] L. J. Rothschild, N. J. H. Averesch, E. A. Strychalski, F. Moser, J. I. Glass, R. Cruz Perez, I. O. Yekinni,

B. Rothschild-Mancinelli, G. A. Roberts Kingman, F. Wu, J. Waeterschoot, I. A. Ioannou, M. C. Jewett, A. P. Liu, V. Noireaux, C. Sorenson, and K. P. Adamala, Building synthetic cells-from the technology infrastructure to cellular entities, ACS Synth. Biol. **13**, 974 (2024).

[7] T. Li, D. Ilhamsyah, B. Tai, and Y. Shen, Functional biomaterials derived from protein liquid–liquid phase separation and liquid-to-solid transition, Adv. Mater. **37**, 2414703 (2025).

[8] T. Yao, C. Feng, and H. Yan, Current developments and applications of smart polymers based aqueous two-phase systems, Microchem. J. **204**, 111170 (2024).

[9] L. Ruiz-Martínez, F. Leermakers, S. Stoyanov, and J. van der Gucht, Tunable capillary suspensions from aqueous two-phase systems, Langmuir **41**, 11604 (2025).

[10] A. Scacchi, C. Rigoni, M. Haataja, J. V. Timonen, and M. Sammalkorpi, A coarse-grained model for aqueous two-phase systems: Application to ferrofluids, J. Colloid Interface Sci. **686**, 1135 (2025).

[11] R. Evans, The nature of the liquid-vapour interface and other topics in the statistical mechanics of non-uniform, classical fluids, Adv. Phys. **28**, 143 (1979).

[12] R. Evans, J. Henderson, D. Hoyle, A. Parry, and Z. Sabeur, Asymptotic decay of liquid structure: Oscillatory liquid-vapour density profiles and the Fisher-Widom line, Mol. Phys. **80**, 755 (1993).

[13] R. Evans, Density functionals in the theory of nonuniform fluids, *Fundamentals of Inhomogeneous Fluids*, edited by D. Henderson, 1st ed. (CRC Press, Boca Raton, 1992).

[14] J. F. Lutsko, Recent developments in classical density functional theory, Adv. Chem. Phys. **144**, 1 (2010).

[15] R. Evans, M. Oettel, R. Roth, and G. Kahl, New developments in classical density functional theory, J. Phys.: Condens. Matter **28**, 240401 (2016).

[16] M. te Vrugt, H. Löwen, and R. Wittkowski, Classical dynamical density functional theory: From fundamentals to applications, Adv. Phys. **69**, 121 (2020).

[17] Y. Rosenfeld, Free-energy model for the inhomogeneous hard-sphere fluid mixture and density-functional theory of freezing, Phys. Rev. Lett. **63**, 980 (1989).

[18] S. M. Oversteegen and R. Roth, General methods for free-volume theory, J. Chem. Phys. **122**, 214502 (2005).

[19] A. J. Archer, B. Chacko, and R. Evans, The standard mean-field treatment of inter-particle attraction in classical DFT is better than one might expect, J. Chem. Phys. **147**, 034501 (2017).

[20] M. Schmidt, H. Löwen, J. M. Brader, and R. Evans, Density functional for a model colloid-polymer mixture, Phys. Rev. Lett. **85**, 1934 (2000).

[21] R. C. Assis, A. B. Mageste, L. R. de Lemos, R. M. Orlando, and G. D. Rodrigues, Application of aqueous two-phase system for selective extraction and clean-up of emerging contaminants from aqueous matrices, Talanta **223**, 121697 (2021).

[22] M. Iqbal, Y. Tao, S. Xie, Y. Zhu, D. Chen, X. Wang, L. Huang, D. Peng, A. Sattar, M. A. B. Shabbir, *et al.*, Aqueous two-phase system (ATPS): An overview and advances in its applications, Biol. Proced. Online **18**, 18 (2016).

[23] C. Rigoni, G. Beaune, B. Harnist, F. Sohrabi, and J. V. Timonen, Ferrofluidic aqueous two-phase system with ultralow interfacial tension and micro-pattern formation, Commun. Mater. **3**, 26 (2022).

[24] T. Furuki, H. Sakuta, N. Yanagisawa, S. Tabuchi, A. Kamo, D. S. Shimamoto, and M. Yanagisawa, Marangoni droplets of dextran in PEG solution and its motile change due to coil–globule transition of coexisting DNA, ACS Appl. Mater. Interfaces **16**, 43016 (2024).

[25] A. S. Holehouse and S. Alberti, Molecular determinants of condensate composition, Mol. Cell **85**, 290 (2025).

[26] L. Verlet and J.-J. Weis, Equilibrium theory of simple liquids, Phys. Rev. A **5**, 939 (1972).

[27] S. Toxvaerd, Perturbation theory for nonuniform fluids: Surface tension, J. Chem. Phys. **55**, 3116 (1971).

[28] D. Henderson, *Fundamentals of Inhomogeneous Fluids*, 1st ed. (CRC Press, Boca Raton, 1992).

[29] J. D. Weeks, D. Chandler, and H. C. Andersen, Role of repulsive forces in determining the equilibrium structure of simple liquids, J. Chem. Phys. **54**, 5237 (1971).

[30] A. A. Louis, P. G. Bolhuis, J. P. Hansen, and E. J. Meijer, Can polymer coils be modeled as "soft colloids"? Phys. Rev. Lett. **85**, 2522 (2000).

[31] P. Bolhuis, A. Louis, J. Hansen, and E. Meijer, Accurate effective pair potentials for polymer solutions, J. Chem. Phys. **114**, 4296 (2001).

[32] C. N. Likos, Effective interactions in soft condensed matter physics, Phys. Rep. **348**, 267 (2001).

[33] I. O. Götze, H. Harreis, and C. Likos, Tunable effective interactions between dendritic macromolecules, J. Chem. Phys. **120**, 7761 (2004).

[34] I. O. Götze, A. J. Archer, and C. N. Likos, Structure, phase behavior, and inhomogeneous fluid properties of binary dendrimer mixtures, J. Chem. Phys. **124**, 084901 (2006).

[35] A. J. Archer and R. Evans, Binary Gaussian core model: Fluid-fluid phase separation and interfacial properties, Phys. Rev. E **64**, 041501 (2001).

[36] A. Scacchi, S. J. Nikkhah, M. Sammalkorpi, and T. Ala-Nissila, Self-assembly in soft matter with multiple length scales, Phys. Rev. Res. **3**, L022008 (2021).

[37] A. Scacchi, M. Sammalkorpi, and T. Ala-Nissila, Self-assembly of binary solutions to complex structures, J. Chem. Phys. **155**, 014904 (2021).

[38] R. Roth, Fundamental measure theory for hard-sphere mixtures: A review, J. Phys.: Condens. Matter **22**, 063102 (2010).

[39] J. M. Brader, R. Evans, and M. Schmidt, Statistical mechanics of inhomogeneous model colloid—polymer mixtures, Mol. Phys. **101**, 3349 (2003).

[40] M. Schmidt, A. R. Denton, and J. M. Brader, Fluid demixing in colloid–polymer mixtures: Influence of polymer interactions, J. Chem. Phys. **118**, 1541 (2003).

[41] H. Reiss, Statistical geometry in the study of fluids and porous media, J. Phys. Chem. **96**, 4736 (1992).

[42] P. B. Warren, S. M. Ilett, and W. C. K. Poon, Effect of polymer nonideality in a colloid-polymer mixture, Phys. Rev. E **52**, 5205 (1995).

[43] R. Melnyk, A. Trokhymchuk, and A. Baumketner, Excluded volume of the system of hard-core spheres revisited: New insights from computer simulations, J. Mol. Liq. **368**, 120672 (2022).

[44] H. N. W. Lekkerkerker, W. C.-K. Poon, P. N. Pusey, A. Stroobants, and P. B. Warren, Phase behaviour of colloid + polymer mixtures, Europhys. Lett. **20**, 559 (1992).

[45] J. F. Lutsko and J. Lam, Classical density functional theory, unconstrained crystallization, and polymorphic behavior, Phys. Rev. E **98**, 012604 (2018).

[46] A. J. Archer, B. D. Goddard, D. N. Sibley, J. T. Rawlings, R. Broadhurst, F. F. Ouali, and D. J. Fairhurst, Experimental and theoretical bulk phase diagram and interfacial tension of ouzo, Soft Matter **20**, 5889 (2024).

[47] See Supplemental Material at http://link.aps.org/supplemental/10.1103/v6nd-87cd for details of the scheme used to determine bulk coexisting densities in a multicomponent, multiphase system, including a flow chart illustrating the procedure for obtaining disjoint solutions of the coexistence equations. It also describes the calculation of inhomogeneous density profiles for a confined fluid mixture and the application of the fast Fourier transform method to evaluate the convolutions required for computing the one-body correlation function, which includes Ref. [65].

[48] A. A. Louis, P. G. Bolhuis, and J. P. Hansen, Mean-field fluid behavior of the Gaussian core model, Phys. Rev. E **62**, 7961 (2000).

[49] J. Rouwhorst, C. Ness, S. Stoyanov, A. Zaccone, and P. Schall, Nonequilibrium continuous phase transition in colloidal gelation with short-range attraction, Nat. Commun. **11**, 3558 (2020).

[50] G. Foffi, G. D. McCullagh, A. Lawlor, E. Zaccarelli, K. A. Dawson, F. Sciortino, P. Tartaglia, D. Pini, and G. Stell, Phase equilibria and glass transition in colloidal systems with short-ranged attractive interactions: Application to protein crystallization, Phys. Rev. E **65**, 031407 (2002).

[51] J. A. Barker and D. Henderson, Perturbation theory and equation of state for fluids. II. A successful theory of liquids, J. Chem. Phys. **47**, 4714 (1967).

[52] M. Farag, W. M. Borcherds, A. Bremer, T. Mittag, and R. V. Pappu, Phase separation of protein mixtures is driven by the interplay of homotypic and heterotypic interactions, Nat. Commun. **14**, 5527 (2023).

[53] A. Kamo, A. Nikoubashman, and M. Yanagisawa, Impact of polydispersity on phase separation: Insights from polyethylene glycol and dextran mixtures, J. Phys. Chem. B **129**, 3263 (2025).

[54] E. Velasco and P. Tarazona, Wetting and drying at a solid-fluid interface, J. Chem. Phys. **91**, 7916 (1989).

[55] E. Bruno, C. Caccamo, and P. Tarazona, Wetting transitions for the Ar-CO 2 interface: Modified-hypernetted-chain and density-functional-theory results, Phys. Rev. A **35**, 1210 (1987).

[56] S. M. Tschopp and J. M. Brader, Fundamental measure theory of inhomogeneous two-body correlation functions, Phys. Rev. E **103**, 042103 (2021).

[57] S. M. Tschopp, H. D. Vuijk, A. Sharma, and J. M. Brader, Mean-field theory of inhomogeneous fluids, Phys. Rev. E **102**, 042140 (2020).

[58] J. R. Edison, N. Tasios, S. Belli, R. Evans, R. van Roij, and M. Dijkstra, Critical Casimir forces and colloidal phase transitions in a near-critical solvent: A simple model reveals a rich phase diagram, Phys. Rev. Lett. **114**, 038301 (2015).

[59] J. R. Edison, S. Belli, R. Evans, R. Van Roij, and M. Dijkstra, Phase behaviour of colloids suspended in a near-critical solvent: A mean-field approach, Mol. Phys. **113**, 2546 (2015).

[60] Y. Ma, D. M. Acosta, J. R. Whitney, R. Podgornik, N. F. Steinmetz, R. H. French, and V. A. Parsegian, Determination of the second virial coefficient of bovine serum albumin under varying pH and ionic strength by composition-gradient multi-angle static light scattering, J. Biol. Phys. **41**, 85 (2015).

[61] M. Schmidt, Rosenfeld functional for non-additive hard spheres, J. Phys.: Condens. Matter **16**, L351 (2004).

[62] A. Härtel, M. Janssen, S. Samin, and R. Van Roij, Fundamental measure theory for the electric double layer: Implications for blue-energy harvesting and water desalination, J. Phys.: Condens. Matter **27**, 194129 (2015).

[63] R. Wittmann, M. Marechal, and K. Mecke, Fundamental measure theory for non-spherical hard particles: Predicting liquid crystal properties from the particle shape, J. Phys.: Condens. Matter **28**, 244003 (2016).

[64] V. A. Varma and A. Scacchi, 2026_VARMA_&_SCACCHI _PRE, Version 1, University of Turku, 2026, https://doi.org/10.23729/fd-9d9fe8df-56ec-3a85-9cb6-802c27786382.

[65] Á. Mulero, *Theory and Simulation of Hard-Sphere Fluids and Related Systems*, Lecture Notes in Physics (Springer, Berlin, 2008), Vol. 753.